Trajectory Optimization for Air-to-Surface Missiles with Imaging Radars

Asif Farooq *

Alenia Marconi Systems Ltd, Borehamwood, Hertfordshire, WD6 1RX, United Kingdom

and

David J.N. Limebeer †

Imperial College, London, SW7 2BT, United Kingdom.

1 Abstract

This paper presents the use of trajectory optimization techniques for the terminal guidance of an air-to-surface missile using a Doppler Beam Sharpening (DBS) radar seeker. The terminal guidance problem is characterized by a stealthy terrain following phase that is followed by a climb and dive onto the target (a "bunt" trajectory). The imaging properties of Doppler Beam Sharpening radars impose additional azimuth plane constraints on the trajectory that have to be incorporated into the optimization process. The various mission phases are inter-related and the performance objectives come into conflict with the hardware constraints. The trajectory optimizer is used to generate off-line open-loop controls that satisfy the various mission requirements. Numerical examples are used to illustrate the method and its efficacy.

*Systems Engineer

†Professor and Head of Department of Electrical and Electronic Engineering

2 Nomenclature

$(R_{sx},\ R_{sy},\ R_{sz})$: *Downrange, crossrange and altitude respectively (m)*

$(V_{sx},\ V_{sy},\ V_{sz})$: *Space frame components of the velocity vector* (ms^{-1})

$(A_{myd},\ A_{mzd})$: *Yaw and Pitch Acceleration demands respectively* (ms^{-2})

$(A_{mx},\ A_{my},\ A_{mz})$: *Body axis accelerations achieved* (ms^{-2})

$(\theta,\ \psi)$: *Pitch and yaw angles (degs)*

$(\lambda_y,\ \lambda_z)$: *Sightline angles in azimuth and elevation respectively (degs)*

$(t_{exp},\ t,\ t_f)$: *Exposure time, current time and final time respectively (s)*

R_b: *Bunt range (m)*

$(\Psi,\ \Theta)$: *Azimuth and elevation look angles respectively (degs)*

$(\alpha,\ \beta)$: *Angles of incidence and sideslip respectively (degs)*

$(\omega,\ \zeta)$: *Bandwidth* $(rads^{-1})$ *and damping ratio of autopilot*

T_i: *Incidence lag (s)*

g: *Acceleration due to gravity* (ms^{-2})

$(\gamma,\ \chi)$: *Flight path and heading angle respectively (degs)*

V: *Total speed* (ms^{-1})

$(p,\ q,\ r)$: *Roll, pitch and yaw rates* $(rads^{-1})$

$(R_{sx}(t_f),\ R_{sy}(t_f),\ R_{sz}(t_f))$: *Target co-ordinates (m)*

T: *Final time calculated by optimizer (s)*

$(R_{sx}(T),\ R_{sy}(T),\ R_{sz}(T))$: *Final position calculated by optimizer (m)*

R_{exp}: *Downrange co-ordinate at which missile crosses exposure height (m)*

Λ: *Angle between target sightline and velocity vector in elevation (degs)*

Ξ: *Angle between target sightline and velocity vector in azimuth (degs)*

Γ: *Impact angle (degs)*

t_b: *Time at which missile becomes exposed (s)*

N: *Number of discretization intervals*

Δ: *Crossrange resolution (m)*

λ: *Wavelength (m)*

$(f_D,\ f_{DA},\ f_{DB})$: *Doppler shifts (Hz)*

δf: *Doppler difference (Hz)*

δt: *Seeker coherent integration period (s)*

R: *Range to go (m)*

J: *Performance index*

$\mathbf{R}$: *Unit vector along sightline axis*

$\mathbf{v}$: *Velocity vector*

$(\mathbf{i},\ \mathbf{j},\ \mathbf{k})$: *Space orientated unit vectors*

Ω: *Total angle between velocity and sightline (degs)*

$f(t)$: *Function for DBS imaging constraint*

$(X_A,\ Y_A,\ Z_A)$: *Sightline frame*

$(X_B,\ Y_B,\ Z_B)$: *Body frame*

$(X_S,\ Y_S,\ Z_S)$: *Earth fixed frame*

$(X_I,\ Y_I,\ Z_I)$: *Missile inertial frame*

$(x,\ y,\ z)$: *Target offset in downrange, crossrange and altitude respectively (m)*

a: *Tuning parameter for imaging state constraint*

Φ: *Scaling parameter used in cost function*

T_{max}: Maximum thrust(N)

C_{do} : Zero incidence drag coefficient

S: Reference area (m^2)

m: Mass of missile (kg)

ρ : Air density (kgm^{-2})

a_0, a_1, a_2: Coefficients for air density polynomial

3 Introduction

This paper considers the use of trajectory optimization techniques for the terminal guidance control of a 5 degree-of-freedom (5DOF) air-to-surface missile with a radar imaging seeker. The terminal guidance phase will typically involve the last minute of flight, at about 15km range, and will require the accurate determination of the target location and information about the optimal approach route to the target. Typically a seeker will be used in conjunction with global positioning satellite (GPS) updates to determine the target location. The seeker uses a high resolution radar image to identify targets at ranges of 10-15km. High resolution in downrange

can be achieved using a narrow transmitted pulse, or by pulse compression techniques and Doppler Beam Sharpening (DBS) processing can be used to achieve high crossrange resolution. This technique requires that an angular offset between the velocity vector and the sightline vector in azimuth and usually gives rise to large crossrange offsets that impose constraints on the trajectory optimization problem. In addition to the imaging requirements, the missile is required to fly at low altitudes to avoid air defense systems. The stealthy approach is followed by a climb and dive (bunt maneuver). This maneuver is used to image the ground area and to achieve a pre-specified impact angle. Impact and incidence constraints are used to maximize the effectiveness of direction sensitive warheads. Optimization in the final phase of flight is of paramount importance, because it is necessary to balance the requirements associated with evading air defenses, satisfying terminal constraints and respecting the missile's dynamic constraints. Conventional methods of guidance such as proportional navigation (PN) have limitations in shaping a trajectory in highly constrained scenarios of this nature.

3.1 Previous research

A lot of work has been done on the trajectory optimization of airborne vehicles. Bunt trajectories that make use of linear optimal control for terminal guidance have been reported in [1] where analytic means are used to determine a state feedback control law. In [2] linear quadratic techniques are used to achieve a terminal angle constraint for re-entry vehicles. Both of these papers deal with the control constraints indirectly via terms in the cost function. An estimate of the time-to-go is needed to compute the feedback gains. There are several advantages associated with control laws that are derived from linear models: (i) they are in a state feedback form, (ii) they can be designed to be robust ([3]) and (iii) they are easy to implement. In [4], the minimum principle is used, along with geometric considerations, to obtain an analytic solution for an air-to-surface missile guidance problem with an impact angle requirement. This paper uses a point mass missile model and a first order lag autopilot with control constraints. The optimal switching instants are determined numerically.

Nonlinear optimal control algorithms in conjunction with point mass models are used in [5] and [6] to study air-to-air scenarios. Reference [5] studies a trajectory synthesis problem for an air-to-air missile with post-stall maneuvering. A receding horizon strategy is used to generate

a feedback mechanism. In [6] open-loop solutions are generated for the range maximization of an air-to-air missile with a fixed final time. The companion paper [7] uses a neighboring optimal control scheme to provide a feedback layer for closed-loop guidance and a proportional navigation (PN) law is used in the terminal phase of flight. Trajectory planning with terrain following for aircraft and helicopters are reported in [8] and [9]. An inverse dynamics approach is employed in [8] to solve a flight time minimization problem with endpoint and terrain clearance constraints. The resulting control law is then implemented using nonlinear predictive control [10].

A more recent approach, that was driven by the continued increases in processor speeds generated the guidance commands by solving a real-time optimization problem. This approach, in conjunction with a point mass model, is also considered in [11] for aircraft range maximization. Singular perturbation techniques are used to reduce the computational burden. Other papers such as [12] and [13] have adapted optimal control algorithms to meet real-time guidance requirements. In [12] collocation is proposed and tested on a number of aerospace examples. Reference [13] compares multiple shooting, direct shooting and collocation for spacecraft closed-loop guidance in terms of reliability and flight processor requirements. Following [13], a guidance algorithm based upon shooting and nonlinear programming is presented in [14] for an advanced launch system. In [15] differential inclusions are used to solve an on-line minimum time to climb aircraft problem using an adaptive node refinement strategy. The nodes are densely placed in the vicinity of the current point and sparsely distributed over the rest of the horizon; the rationale being that the optimal control sequence should be based predominantly on local behaviour. Simulations were then carried out to compare the on-line solution with a more accurate off-line solution.

On-line approaches have the advantages of being autonomous and are less reliant on extensive preflight analysis. If the terminal boundary conditions are modified substantially, or disturbances cause large deviations from a nominal preflight trajectories these methods become even more attractive. Linear approximations for trajectory tracking are not needed and mission flexibility may be enhanced. This adaptive guidance capability may be particularly important in the context of missile control problems, where uncertainties in target position and aerodynamic data as well as new mission data call for the repeated regeneration of trajectory profiles.

3.2 Current Research

Trajectory optimization studies for a simple missile autopilot/airframe model are presented. Our terminal guidance problem is characterized by pathwise state constraints (representing in-flight constraints), terminal equality constraints, control bounds and a free final time. Numerical means are used to determine open-loop optimal trajectories. These open-loop optimal trajectories are useful both as a benchmark for design purposes and can potentially be used as part of a closed-loop implementation.

A five degree-of-freedom (5DOF) model that is described in Section 4 will be used in conjunction with a quadratic autopilot/airframe representation for the pitch and yaw freedoms. The calculation of optimal trajectories for the terminal guidance problem is essentially a nonlinear constrained optimization problem for which a multitude of techniques can be used. These range from the conventional (gradient and shooting methods) to more recent optimization algorithms. Obvious difficulties arise from conflicts between some of the objectives and constraints in the optimal control formulation of the terminal guidance problem. The model is given as a set of dynamic equations and an objective function is minimized subject to pathwise state constraints, control bounds and terminal trajectory constraints.

An optimization toolbox based on the algorithms described in the papers [17], [18], [19] and [20] and in the book [21] is used. The toolbox consists of a FORTRAN implementation of a sequential quadratic programming algorithm, specifically tailored to solve optimal control problems with state constraints. The optimization algorithm is coupled to an adaptive step size integration scheme for differential-algebraic systems. Convergence analysis and comparisons with other optimization packages on some sample optimal control problems can be found in [21]. In the current problem, the physical limits likely to be encountered such as look angle, "g-capability" and incidence constraints are dealt with naturally by this optimal control method. They are essentially state and control constraints. The control inputs to the system are the pitch and yaw acceleration demands. By invoking a discretization scheme and an appropriate parameterization of the controls, trajectories that satisfy both the bunt and imaging requirements can be generated. The trajectories calculated for each test case will satisfy the necessary conditions for optimality, but they may not correspond to a global minimum. It turns out that there are multiple minima and guaranteeing a global minimum is complex,

computationally demanding and possibly unnecessary. The extent to which the objectives are balanced depends critically on the scaling factors used in the problem. A description of the way in which the terminal guidance requirements are formulated and the scaling factors used is described in Section 5. Section 6 presents the results for two test cases with varying impact angle requirements. Conclusions are drawn in Section 7.

3.3 Terminal Guidance Problem and Method of Solution

The central requirements of the terminal guidance problem are to minimize both the miss distance and the exposure time to air defense systems. For direction sensitive warheads, a requirement in the elevation plane is the ability to hit the target at a specified impact angle (this is measured from a vertical reference). The ideal case corresponds to a zero impact angle and is commonly referred to as a "vertical" impact. The impact angle requirement is scenario dependent and, in the case of soft targets, may be relaxed. In many cases, the impact angle requirement necessitates a bunt maneuver of some kind. During the climb phase of the bunt, it will be necessary to image the target to determine its exact location. This data will be used to make final adjustments to the trajectory. The trajectory optimization problem has to incorporate several constraints including: (i) the vehicle's lateral acceleration capability, (ii) radar imaging constraints, (iii) the seeker look angle constraints and (iv) the ground clearance. These constraints determine the height needed to obtain a pre-specified impact angle and the range required to perform the bunt maneuver.

Radar imaging guidance introduces an interesting control constraint, because it requires an azimuth squint angle in order to enhance the cross-range resolution of the image. These details are covered in Appendix A. Unlike the other constraints, the radar imaging constraints cannot be implemented simply as control or state constraints. The difficulties arise from the fact that the offset requirements associated with the radar come into conflict with the terminal constraints. One cannot simultaneously maintain a cross-range offset throughout the flight as the missile must commence terminal homing at some range to go.

4 Model

The system equations were derived for a symmetric skid-to-turn (STT) missile which is assumed to be roll stabilized. The model assumes that controllers for both the pitch and the yaw autopilots have been implemented and that the closed-loop autopilot/airframe characteristics can be represented by quadratic responses. This is a reasonable approximation for the closed-loop missile dynamics if higher frequency effects such as actuator dynamics and non-minimum phase effects can be neglected as shown in [16]. Euler angles are used in the body-to-space transform — this means that zero impact angles cannot be achieved due to singularities. However, small non-zero impact angles can be specified and achieved without difficulty. Additional assumptions are:

1. The missile is roll stabilized so that the roll angle is small enough to be neglected.
2. The antenna and sightline frames are coincident (i.e. the seeker is pointing at the target throughout the flight). It is assumed that the target co-ordinates are known in advance and that the seeker is stabilized against body motion coupling effects.
3. The sightline and antenna frames do not roll.
4. The target is stationary.
5. Modeling errors and exogenous disturbances are neglected.
6. The terrain is flat and level.
7. The engine thrust is constant.
8. A zero incidence drag term is used to calculate the drag force.
9. The target has been acquired and recognized prior to the terminal guidance phase.

On the basis of these assumptions, the system equations can be written in state-space form:

$$\dot{R}_{sx} = V_{sx} \tag{1}$$

$$\dot{R}_{sy} = V_{sy} \tag{2}$$

$$\dot{R}_{sz} = V_{sz} \tag{3}$$

$$\dot{V}_{sx} = cos(\theta)cos(\psi)(A_{mx}) - sin(\psi)(A_{my}) - sin(\theta)cos(\psi)(A_{mz}) \quad (4)$$

$$\dot{V}_{sy} = cos(\theta)sin(\psi)(A_{mx}) + cos(\psi)(A_{my}) - sin(\theta)sin(\psi)(A_{mz}) \quad (5)$$

$$\dot{V}_{sz} = sin(\theta)(A_{mx}) + cos(\theta)(A_{mz}) \quad (6)$$

$$\ddot{A}_{my} = -2\zeta\omega(\dot{A}_{my}) - \omega^2(A_{my}) + \omega^2(A_{myd}) \quad (7)$$

$$\ddot{A}_{mz} = -2\zeta\omega(\dot{A}_{mz}) - \omega^2(A_{mz}) + \omega^2(A_{mzd}) - \omega^2 g\ cos(\theta) \quad (8)$$

$$\dot{\theta} = \frac{A_{mz} + T_i(\dot{A}_{mz})}{V} \quad (9)$$

$$\dot{\psi} = \frac{A_{my} + T_i(\dot{A}_{my})}{V\ cos(\theta)} \quad (10)$$

$$V = \sqrt{{V_{sx}}^2 + {V_{sy}}^2 + {V_{sz}}^2} \quad (11)$$

$$A_{mx} = \frac{T_{max}}{m} - g\ sin(\theta) - \frac{\rho\ V^2 S C_{do}}{2m} \quad (12)$$

$$\rho = a_0 + a_1 R_{sz} + a_2 {R_{sz}}^2 \quad (13)$$

$$\gamma = sin^{-1}\left(\frac{V_{sz}}{V}\right) \quad (14)$$

$$\chi = tan^{-1}\left(\frac{V_{sy}}{V_{sx}}\right). \quad (15)$$

The air density variation with altitude is modeled by a second order polynomial and is based upon the atmosphere model provided in [22]. The missile's aerodynamic drag is approximated by a zero incidence drag term. The parameters below are deemed to be representative of a conventional closed-loop autopilot design at a nominal flight condition:

$$\omega = 10\ rads^{-1},\ \zeta = 0.7,\ T_i = 0.5s \quad (16)$$

$$m = 500kg, T_{max} = 2500N, C_{do} = 0.3, S = 0.132m^2 \quad (17)$$

$$a_0 = 1.224, a_1 = -1.142d^{-4}, a_2 = 3.312d^{-9} \quad (18)$$

$$|\ A_{myd},\ A_{mzd}| \leq 80ms^{-2}. \quad (19)$$

The two controls are the normal acceleration demands (A_{myd} and A_{mzd}), which are parameterized using piecewise constant functions with 400 intervals each. The missile initial conditions are shown in Table 1. The initial conditions describe a missile with an initial height of 30m above the ground, and a longitudinal speed of $306ms^{-1}$ (Mach 0.9 at sea level). The missile is assumed to be flying straight and level.

$R_{sx}(0) = 0m, R_{sy}(0) = 0m, R_{sz}(0) = 30m$
$V_{sx}(0) = 306ms^{-1}, V_{sy}(0) = 0ms^{-1}, V_{sz}(0) = 0ms^{-1}$
$A_{my}(0) = 0ms^{-2}, A_{mz}(0) = 0ms^{-2}, \dot{A}_{my}(0) = 0ms^{-3}, \dot{A}_{mz}(0) = 0ms^{-3}$
$\theta(0) = 0^o, \psi(0) = 0^o, \gamma(0) = 0^o, \chi(0) = 0^o$

Table 1: Missile Initial Conditions

4.1 Further Definitions

A number of performance measures will be used to quantify the optimal trajectories. Denoting $R_{sx}(T)$, $R_{sy}(T)$ and $R_{sz}(T)$ as the terminal downrange and altitude calculated by the optimizer and $R_{sx}(t_f)$, $R_{sy}(t_f)$ and $R_{sz}(t_f)$ as the target position, the total miss distance is therefore:

$$Total\ miss = \sqrt{(R_{sx}(T) - R_{sx}(t_f))^2 + (R_{sy}(T) - R_{sy}(t_f))^2 + (R_{sz}(T) - R_{sz}(t_f))^2} \tag{20}$$

This is the miss distance computed when the integration algorithm stops and not the point of closest approach. The impact angle is defined as the trajectory slope at the final time and can be determined either from the space components of the velocity vector, or the flight path angle:

$$\Gamma = tan^{-1}\left(\frac{V_{sx}(T)}{V_{sz}(T)}\right) = 90 - |\gamma(T)| \tag{21}$$

The exposure time is defined as the difference between the time the missile crosses a certain threshold height (100m say), denoted as t_b and the final time (T) calculated by the optimizer. The threshold height is assumed to be the height at which the missile becomes exposed to air defense systems and is otherwise arbitrary. This is shown in two dimensions in Figure 1; the exposure time is therefore:

$$t_{exp} = T - t_b. \tag{22}$$

The bunt range is calculated as the difference between the target ground plane co-ordinates and the ground plane co-ordinates at which the missile crosses the exposure height threshold. Denoting the latter by $R_{sx}(t_b)$ and $R_{sy}(t_b)$, the bunt range is:

$$R_b = \sqrt{(R_{sx}(t_f) - R_{sx}(t_b))^2 + (R_{sy}(t_f) - R_{sy}(t_b))^2}. \tag{23}$$

The distance-to-go co-ordinates are given by:

$$x \quad = \quad R_{sx}(t) - R_{sx}(t_f) \tag{24}$$

$$y = R_{sy}(t) - R_{sy}(t_f) \tag{25}$$

$$z = R_{sz}(t) - R_{sz}(t_f). \tag{26}$$

The range to the target is therefore:

$$R = \sqrt{x^2 + y^2 + z^2}. \tag{27}$$

and the pitch and yaw sightline angles are defined as:

$$\lambda_z = sin^{-1}\left(\frac{z}{R}\right) \tag{28}$$

$$\lambda_y = tan^{-1}\left(\frac{y}{x}\right). \tag{29}$$

The calculation of the seeker look angles can be shown to be (we denote cos(·) by $c(\cdot)$, sin(·) by $s(\cdot)$, $cos^{-1}(\cdot)$ by $c^{-1}(\cdot)$ and $sin^{-1}(\cdot)$ by $s^{-1}(\cdot)$):

$$\Psi = c^{-1}\left(s(\lambda_y)s(\psi) + c(\lambda_y)c(\psi)\right) \tag{30}$$

$$\Theta = c^{-1}\left(s(\lambda_z)c(\lambda_y)s(\theta)c(\psi) + s(\lambda_y)s(\lambda_z)s(\theta)s(\psi) + c(\lambda_z)c(\theta)\right). \tag{31}$$

Similarly, the angles between the sightline and velocity vector in azimuth and elevation can be shown to be:

$$\Xi = c^{-1}\left(s(\lambda_y)s(\chi) + c(\lambda_y)c(\chi)\right) \tag{32}$$

$$\Lambda = c^{-1}\left(s(\lambda_z)c(\lambda_y)s(\gamma)c(\chi) + s(\lambda_y)s(\lambda_z)s(\gamma)s(\chi) + c(\lambda_z)c(\gamma)\right). \tag{33}$$

The time for the terminal guidance run is defined as the time-to-go when the range to the target is less than 2km. This is the time/range at which the radar imaging data would facilitate a reversion to another guidance method, since it is not possible to image and home in on the target at very short ranges.

5 Optimal Control Formulation

Attention is now turned to the way in which the DBS and bunt requirements are embedded in an optimal control problem. The detailed choice of the cost function and the problem scaling factors have a major influence on the solution. In order to achieve adequate crossrange resolution from DBS radar imaging a minimum value of angle in azimuth has to be maintained

between the missile velocity vector and the sightline vector from the missile to the target. Some means of translating this into a form suitable for optimization is required. The generation of optimal trajectories can be envisaged as a multi-objective optimization problem in which some of the objectives (e.g. miss distance) take precedence over others. The problem needs to be carefully formulated and scaled to ensure that the optimal controls take account of all the (conflicting) problem requirements, some of which are listed below:

- The minimization of the miss distance
- The minimization of the exposure time
- The minimization of the maximum height
- The minimization of the impact angle
- The maintenance of a sufficient angular offset for radar imaging purposes
- Keeping the target in view throughout bunt maneuver — seeker look angle constraints
- The maintenance of adequate ground clearance during terrain following
- Ensuring that none of the missile's physical limits are exceeded during the bunt maneuver
- Smooth controls for both autopilots that are easy to implement.

Many of the trade-offs are scenario dependent. For instance, the requirement of steep impact angles may be less important for soft targets in which case the exposure time could be reduced. In the case of systems using global positioning satellites (GPS), it is possible that the elevation look angle constraint can be relaxed as it may be possible for the target to move out of view for a fraction of the flight. These trade-offs are essentially "balanced" by the scaling factors introduced in the optimal control formulation. It is generally difficult to determine whether a set of terminal conditions is feasible, given the physical constraints (for example: g-capability and look angle limits). The approach taken here is to specify a relaxed set of requirements and use this as a basis for approaching more stringent performance specifications. When issues of robustness are considered, it may well be preferable to sacrifice some performance by using a relaxed formulation. The crossrange resolution obtained using DBS processing can be shown

to be (see Appendix A):

$$\Delta = \frac{R\lambda}{2V(\delta t)sin(\Xi)\ cos(\Lambda)}. \tag{34}$$

Note that the crossrange resolution is inversely proportional to sin (Ξ). For optimization purposes the following approximation was used for the crossrange resolution:

$$\Delta \approx \frac{\lambda\,(x^2+y^2)}{2V(\delta t)y} \tag{35}$$

because it is better behaved numerically than the true expression (34). The difficulty with (34) stems from the fact that (Ξ) and (Λ) are complicated functions of the body attitude and the sightline angles and this can result in numerical difficulties when Ξ is small or Λ is near 90 degs. With the crossrange resolution and model equations specified, the optimal control problem is now formulated. In order to control the missile height and crossrange position, the following performance index was investigated:

$$J = \int_0^T \left((R_{sz}-20)^2 + \Phi(R_{sy})^2\right)\ dt. \tag{36}$$

The first term effectively penalizes altitude deviations from a reference datum of 20m. The second term penalizes substantial deviations in crossrange and is used to "encourage" a large crossrange offset; the weighting factor (Φ) is constant. In summary, minimizing the cost function reduces exposure to air defense units (ADUs), through the first term, while the second term maintains a high DBS crossrange resolution. In reality, this is a somewhat simplistic portrayal as detection would be dependent on other factors such as the aspect angle, range to an ADU and the radar cross section (RCS) of the missile. These issues are disregard. The following terminal equality constraints are also prescribed:

$$R_{sx}(t_f) = 15000m \tag{37}$$

$$R_{sy}(t_f) = 5000m \tag{38}$$

$$R_{sz}(t_f) = 20m \tag{39}$$

$$\gamma(t_f) = -70\ degs \tag{40}$$

$$\theta(t_f) = -70\ degs. \tag{41}$$

These constraints specify the terminal position co-ordinates and the elevation angles at impact. These figures are based on estimates of the terminal guidance phase of a typical mission, which

would start at 15-20km from the target. It is more difficult to estimate the crossrange offset: we choose a 5km offset for this problem, since this figure, from the initial geometry, does not transgress any azimuth look angle constraints. It also results in an initial crossrange resolution of less than 2.5m, for realistic values (0.3s to 0.5s) of the seeker coherent integration period (δt), which should be sufficient for target acquisition and recognition (See Assumption 9 in Section 4). Other crossrange offsets can be imposed without difficulty. In the most extreme case there would be no offset and the missile may have to move away from the target in the azimuth plane, while not violating any seeker look angle constraints. This would enable the seeker to form a high resolution image of the terrain, before homing in, but is potentially a more difficult problem as the initial crossrange resolution may be poor. The fact that the flight path and body attitude at impact are required to be the same value effectively minimizes any incidence at impact. All of the above are hard constraints and require accurate controls. State constraints on the seeker azimuth and elevation look angles are also specified. The antenna is typically gimballed, and this constraint is necessary to prevent the antenna servo from operating at its limit and to keep the target within the seeker field of view:

$$\Theta(t) \geq -40 \ degs \qquad \forall t \in [0, T] \tag{42}$$

$$\Psi(t) \leq 40 \ degs \qquad \forall t \in [0, T]. \tag{43}$$

The elevation look angle is negative as the missile is above the target. During the descent phase of the bunt maneuver, the elevation look angle steadily decreases to zero as the sightline and body axes become aligned. Similarly, from the initial geometry, the azimuth look angle is positive and should remain positive, with a gradual reduction to zero near the impact point. Simulations confirmed that at this stage, these constraints need only to be imposed in one direction. A ground clearance constraint is required to prevent a ground plane collision. We used:

$$R_{sz}(t) \geq 10m \qquad \forall t \in [0, T]. \tag{44}$$

Since the target aim off point is 20m above the ground the state constraint (44) is not in conflict with the terminal z-position requirement (39). The case where the target is at ground level can also be accommodated, but it requires a slightly more complicated function for the state constraint (e.g. a function that is offset by 10m and decreases rapidly near the terminal downrange). There may be advantages in selecting an aim off point above the target and

switching to a closed-loop guidance law during the final few seconds of flight.

The DBS imaging requirements are for high resolution imaging up to the terminal guidance run. This facilitates the accurate selection of an aimpoint on the target at the point of handover. It should be recognized that large crossrange offsets do not always provide good crossrange resolution. This follows from the fact that the missile's velocity and the sightline vectors can be closely aligned even if there is a large crossrange offset. With this in mind, the DBS constraints were enforced via an additional state constraint that makes use of the approximate crossrange resolution expression (35). We choose a suitable function, in this case an exponential, which specifies the minimum crossrange resolution as a continuous function of the crossrange co-ordinate. The DBS constraints are then handled by this one additional state constraint. Our choice of function is as follows:

$$f(t) = 0.1 + 2.6\ exp\left(\frac{-R_{sy}}{a}\right),\ a = 800. \tag{45}$$

The a-parameter controls the tradeoff between high resolution imaging and the bunt characteristic — a low value of (a) emphasizes imaging. In contrast, a high value of (a) will put less emphasis on imaging and the trajectory in the azimuth plane will be similar to that associated with proportional navigation (PN). The imaging constraint is therefore:

$$\Delta - f(t) \leq 0.0 \qquad \forall t \in [0, T]. \tag{46}$$

5.1 Choice of Initial Controls and Final Time

The optimal control problem can be re-cast as a nonlinear programming problem by parameterizing the controls and discretizing time. To facilitate rapid convergence we also require sensible estimates for the final time and the initial controls. The choice of the first control (for the pitch autopilot) is straightforward and is chosen for straight and level flight. Since gravity is included, we have:

$$A_{mzd}(t) = 9.81 ms^{-2} \qquad \forall t \in [0, T]. \tag{47}$$

The second control (for the yaw autopilot) and the final time are dependent upon the range to the target. Based on the initial geometry, and initial missile speed, we can calculate the following under-estimate for the final time:

$$T \geq \frac{\sqrt{15000^2 + 5000^2}}{306} = 52\ s. \tag{48}$$

since the bunt maneuver will increase the total flight time. Since the thrust and drag tend to cancel one another, a constant speed approximation of $306ms^{-1}$ is not an unreasonable one. We used this value as the initial estimate of the final time. Finally, it is necessary to provide an estimate for the initial yaw control that will negate the $5km$ crossrange offset. From elementary mechanics, the crossrange offset can be written:

$$y = \frac{1}{2} A_{myd} T^2. \tag{49}$$

Substituting the values for the final time and the crossrange offset and rounding up:

$$A_{myd}(t) = 4.0ms^{-2} \qquad \forall t \in [0, T]. \tag{50}$$

It turns out that these initial controls and final time takes the missile close to the terminal position on the first iteration, but neither the imaging requirement nor the impact angle requirements are satisfied.

5.2 Scaling Factors

In order to balance the conflicting requirements in the constrained optimal control problem it is usually necessary to introduce some scaling. The initial choice of controls: $A_{myd} = 4ms^{-2}$ and $A_{mzd} = 9.81ms^{-2}$ ensure that the constraint violations in each of the three terminal position variables will be of roughly equal order. This choice of initial controls will also cause the missile to hold its initial height. For these reasons, the weightings on the three terminal position constraints were chosen equal. By the same token, the ground clearance state constraint was given a unity weight. The remaining quantities, some of which are angles expressed in radians, require increased emphasis. The multipliers shown in Table 2 were found by trial and worked well in the examples:

Constraint	Scaling Factor
Terminal x position	1.0
Terminal y position	1.0
Terminal z position	1.0
Terminal body attitude	1000.0
Terminal flight path angle	1000.0
Ground clearance state constraint	1.0
DBS imaging state constraint	100.0
Seeker elevation look angle constraint	100.0
Cost function	10^{-6}

Table 2: Scaling factors

5.3 Method of Solution

The common numerical techniques for solving an optimal control problem are the so-called direct and indirect techniques. Indirect techniques are known to be highly accurate, but require substantial pre-analysis and may be difficult to apply to complex problems. In this study a direct method was used. Direct methods discretize time, the states and the controls and use some functional approximation for the control variables (e.g. piecewise constant functions or splines). In this way, the original problem can be recast as a nonlinear programming problem. Full discretization involves parameterizing both the states and controls by via a collocation scheme and the associated state and control parameters are treated as "unknowns". An alternative method (sometimes called direct shooting), which results in a smaller sized problem, is to determine the states recursively using a search in the control space. Both methods result in a finite dimensional nonlinear programming problem. Solutions can be obtained by applying a nonlinear programming algorithm such as sequential quadratic programming.

In this study the direct shooting method was employed and the controls are parameterized using piecewise constant functions. For example the pitch control is represented as:

$$Amzd(t) = \sum_{i=1}^{N} p_i(t) Amzd_i \quad \forall t \in [0, T], i = [1, 2...N] \tag{51}$$

in which the $Amzd_i$'s are constants and $p_i(t) = 1.0, t_i \leq t \leq t_{i+1}$ and 0 elsewhere. The t_i's

are all the same and given by T/N. A similar parameterization is applied for the yaw control. The states are determined using a Radau IIA integration algorithm for differential-algebraic systems (see [21]) for further details). Gradients are determined by the backward integration of an adjoint system of equations. The $Amzd_i$'s are then adjusted at each iteration using a sequential quadratic programming algorithm in order to minimize the cost function and satisfy the constraints. Table 3 shows the values which were used for the convergence criteria, the integration tolerances and the number of discretization intervals:

Number of intervals for each control	400
Integration absolute tolerance	10^{-3}
Integration relative tolerance	10^{-3}
Convergence criteria	10^{-5}

Table 3: Optimization parameters

This means that, for any solution, all the constraints are satisfied with a tolerance of 10^{-5}. As explained in [21], approximation errors can be eliminated by reducing the integration tolerances and re-running the optimization algorithm with the converged control as the initial guess (this is similar to grid refinement techniques). For the results in this study, this refinement step was not carried out as the solutions obtained were already thought to be sufficiently accurate for our purposes. In this study the computations were performed using double-precision arithmetic on a Sun SPARC workstation.

6 Results

Results are given for two test cases with different impact angles. These studies will serve to reenforce the use of optimal control ideas in this type of work as well as illustrate the sensitivity of the solution to the impact angle specification. In the same way, other performance parameters such as the bunt range and the maximum height can also be examined in conjunction with the DBS imaging requirements. We assume the following value for the K-band radar wavelength:

$$\lambda = 0.0085m. \tag{52}$$

and the following range of values are assumed for the seeker coherent integration period:

$$0.3s \leq \delta t \leq 0.5s. \tag{53}$$

Three discrete values of integration period will be considered (0.3s, 0.4s and 0.5s) and the results compare the effect of varying this parameter. A larger value of (δt) corresponds to an increased synthetic diameter with a corresponding improvement in crossrange resolution. As explained in Appendix A, it is impossible to perform DBS imaging on the target throughout the engagement and so a final guidance phase must be used to home in on the target when the crossrange resolution degrades. For these reasons we assume that at a certain range from the target (approximately 2km) the missile switches from DBS mode to a conventional guidance method as beyond this range there is an increased level of conflict between imaging and terminal guidance. A high resolution image of the target near this range will be required. Our results confirm that a range of 2km is sufficient for adequate crossrange resolution, without compromising the terminal guidance requirements of small miss distances and terminal angle constraints.

In the first case (Case A) we specify a terminal impact angle of 20 degs— this is sufficient for some targets. The constraints and cost function are those described in Section 5. Figure 2 shows the optimal trajectory in 3D as well as its projection onto the ground plane. This shows that the missile follows a "ground hugging" trajectory for over 10km before the commencement of the bunt maneuver which begins at approximately 10km downrange and 1.7km crossrange. The crossrange, altitude and optimal controls are shown in Figure 3. In each case these quantities are expressed as functions of the downrange. The azimuth angle between the velocity and sightline as well as the crossrange resolution, for three values of DBS integration period, are shown in Figure 4 as a function of the "range-to-go".

In the second case (Case B), the impact angle is changed in order to examine the sensitivity of the solution to a more demanding specification in this terminal performance parameter. We would expect there to be some conflict between achieving a small impact angle, whilst performing high resolution imaging. The following constraints are modified (as compared with case A).

$$\gamma(t_f) = -85\ degs \tag{54}$$

$$\theta(t_f) = -85\ degs. \tag{55}$$

The other constraints remain unchanged. It can be seen from the 3D plot of the trajectory in Figure 5 that the terrain following phase occupies the first 10km of downrange and the bunt maneuver begins immediately thereafter. In this case the peak height increases to just over 1300m. The state trajectories and controls are shown in Figure 6. The overall performance for the two test cases is shown in Table 4.

Performance Measure	Case A	Case B
Miss distance(m)	1.08 x 10^{-5}	4.59 x 10^{-6}
Time for terminal guidance run(s)	7.39	7.89
Maximum height(m)	1168	1327
Exposure time(s)	21.0	21.89
Bunt range(m)	5184	5073
Impact angle (degs)	20.0	5.0
Incidence at Impact (degs)	0.0	0.0
Maximum azimuth look angle (degs)	24.7	24.9
Maximum elevation look angle (degs)	33.52	39.33
Max g (pitch)	3.56/-5.47	3.79/-6.77
Max g (yaw)	2.44/-0.03	2.50/-0.15
Impact speed (ms^{-1})	305	297
Final time (s)	56.68	57.96

Table 4: Performance comparison

6.1 Analysis of results

Table 4 shows that in both cases all the terminal constraints are satisfied with no state constraint violations. Figures 3 and 6 show that the pitch control maintains its $9.81ms^{-2}$ upward acceleration demand for straight and level flight until the bunt range is reached. At this point, following a brief dip, the pitch acceleration demand increases thereby forcing the missile into a steep climb. There then follows a decrease in the normal acceleration demand to turn the missile over at the apogee and a accelerate it into the target. The maximum negative acceleration

demand is required near the final time. The pitch control experiences a return to near zero demand at the final time in order to "wash out" any pitch plane incidence. In the azimuth plane very little yaw control is used in the first 10km of downrange. There then follows a gradual increase to a maximum value of ($23.94ms^{-2}$ in Case A compared with $24.53ms^{-2}$ in Case B). This is used to align the velocity and sightline vectors in azimuth and to satisfy the terminal requirements. The controls are relatively smooth for both test cases. For Case B the 15 degs tightening in the impact angle requires around 160m of extra height, a increase in flight time and a slight increase in exposure time. The seeker elevation look angle is increased by around 6 degs to 39 degs and the maximum acceleration demand for the pitch autopilot is increased by approximately $12.75ms^{-2}$. The increase in the bunt height reduces the impact speed by approximately $8ms^{-1}$. Although a lower speed during the bunt increases vulnerability, this speed reduction can be used to increase the rate of turn (see equation [9]).

The azimuth angle between the velocity and sightline and the crossrange resolution (for various DBS integration periods) are plotted against range-to-go in Figures 4 and 7. It can be seen from these diagrams that the angle between the sightline and velocity vector in azimuth has a maximum at approximately 4km range-to-go for both test cases, before decreasing to approximately 10 degs at 2km in range-to-go. Each choice of integration period has a minima for the crossrange resolution at roughly 3km range-to-go. As explained in the Appendix, this is a necessary consequence of the terminal constraints. To home in on the target, the velocity and sightline vectors must become aligned at some range-to-go. As the angular offset in azimuth reduces, the crossrange resolution will increase. The velocity vector and sightline vector in azimuth become aligned approximately 600m from the target. This is not shown in any of the figures due to the singularity at this point. The crossrange resolution starts to increase rapidly at a range of around 1.5km as this singularity is approached. The final time is increased by roughly 6.0s from our initial guess and further simulations show this increase is principally due to the DBS imaging requirement, rather than the bunt maneuver. In other words, the need to maintain a large crossrange offset increases the flight time. In terms of the imaging requirements at 2km range, the crossrange resolution for both the test cases is stated in Table 5 for various values of the DBS integration period. For case A, at 2km range-to-go, the crossrange resolution is 0.61m for the integration period of 0.3s, improving to 0.36m for an integration period of 0.5s. For Case B there is a slight degradation in crossrange resolution as a function of range-to-go;

Case	Resolution at 2km, $\delta t = 0.3s$	Resolution at 2km, $\delta t = 0.4s$	Resolution at 2km, $\delta t = 0.5s$
A	0.61m	0.46m	0.36m
B	0.70m	0.53m	0.42m

Table 5: Crossrange resolution at 2km for various DBS integration periods

this is due to the increase in the maximum height. The degradation is more marked for the smaller integration period of 0.3s. Ideally, the crossrange resolution would be sufficient at 2km for aimpoint optimization, though this is dependent on factors outside of trajectory control. The lower integration period of 0.3s may require DBS imaging to a shorter range than 2km in both test cases, which may run into conflict with the terminal guidance requirements. Similarly, for Case B, the crossrange resolution for the integration period of 0.4s may need to be improved. This could be done by tightening the radar imaging specifications further in the optimization process. Again, this is likely to impinge on the constraints in the elevation plane. We would expect the exposure time to be increased (as an azimuth offset may need to be maintained for a longer period) and the bunt trajectory to be altered. Given that the maximum acceleration used is well within the limits imposed, further performance improvements may be possible. It is somewhat surprising that more control effort is not used in the azimuth plane where a large acceleration correction may be needed to home in on the target, this appears to be due to the fact that the azimuth angle between the velocity and sightline is gradually reduced to zero in order to hit the target, with a resultant smooth control action.

In summary, the bunt maneuver with the tighter performance specification associated with Case B is achievable without a significant degradation in exposure time. With that said, the physical constraints on the missile hardware are significantly increased with 1g of extra pitching capability as well as an increased seeker elevation look angle. When disturbances and modeling errors are considered, these hardware specifications may well escalate further. In terms of imaging, seeker coherent integration periods of 0.5s and 0.4s would be acceptable for both cases as both these integration periods are able to achieve acceptable crossrange resolution at a range of 2-3km. For the lowest value of seeker integration period (0.3s) further optimization may be required to achieve lower values of crossrange resolution, requiring a more aggressive

trajectory in the azimuth plane.

7 Conclusions

The paper addresses the problem of calculating optimal controls for a missile with a radar imaging seeker using Doppler Beam Sharpening. The problem requirements are translated into an optimal control problem that can then be solved using numerical optimization. Optimal controls were sought that "balance" the problem tradeoffs including low exposure times, steep impact angles and high resolution imaging. By applying a trajectory optimization method, we were able to calculate trajectories that allowed a high resolution radar image to be formed, thereby enabling target detection, recognition and aimpoint selection. Various values of the seeker coherent integration period were examined to determine the sensitivity of the imaging capability to this parameter. Two test cases were examined with different impact angle requirements. By comparing the two cases, it can be seen that the optimal controls exhibit a predictable structure: the pitch control builds to a peak positive acceleration demand that is followed by the gradual use of a negative acceleration demand that turns the missile at the apogee. A return to zero control at the final time is necessary to minimize the incidence at impact. The yaw acceleration demand requires less control effort (under 3g) by virtue of the problem geometry. With that said, it is conceivable that an increase in maximum lateral control effort could be used to improve further the crossrange resolution thereby producing a sharper turn in the azimuth plane. Seeker coherent integration periods of 0.4s and 0.5s are acceptable in terms of achieving high crossrange resolution at ranges of 2-3km for target aimpoint selection. The results show that steeper impact angles compromise the crossrange resolution, as well as requiring an increase in the maximum height, the maximum elevation look angle and the total flight time. Despite this, the solutions obtained achieve an acceptable compromise between the various performance specifications such as high resolution imaging, low exposure times and low impact angles without transgressing any realistic physical limits. In a practical situation it is advisable to leave some "slack" in the in-flight constraints and some additional control authority as noise and modeling errors must be accommodated.

8 Acknowledgements

The results in this paper were supported by funding from Alenia Marconi Systems Ltd.

9 Appendix A: Doppler Beam Sharpening Equations

Doppler Beam Sharpening is a form of synthetic aperture radar which can be used to obtain high crossrange resolution. The equations needed to represent the Doppler beam sharpening concept used for radar imaging are detailed in this section. A more detailed description of synthetic aperture radar and the associated radar signal processing may be found in chapter 7 of [23], pages 616-652 in [24] and [25]. We derive the relevant Doppler beam sharpening equations to use in the optimal control formulation using basic radar principles and the problem geometry. Difficulties inherent in Doppler beam sharpening radars such as motion compensation, speckle, the signal processing and the target detection and recognition are not considered in this paper. Some of these details can be appended at a later stage, but the main purpose of this paper is to consider the geometric constraints Doppler beam sharpening radars impose on the trajectory optimization problem and the way in which these constraints interact with the overall terminal guidance problem.

Consider the scenario shown in Figure 8 where a missile using a radar imaging seeker is flying at a fixed height above the ground with the antenna beam illuminating an area on the ground. The downrange resolution is determined by the transmitter pulse width. Narrow pulses, or longer pulses, which use pulse compression techniques, result in fine downrange resolutions. For high crossrange resolution a large antenna diameter can be synthesized by storing and processing pulses over an appropriate length of the flight path. The processing requires amplitude and phase information to be stored from each scatterer to form a radar image of the ground area, which can be used to form a narrow synthetic beam. During the seeker coherent integration period, pulse returns can be resolved into a number of Doppler frequencies (as they have different Doppler shifts). This enables a high resolution image of the ground area to be formed. For terminal guidance purposes finer resolution cells are required as the engagement proceeds for target detection and recognition. The limiting factor is the crossrange resolution, which can be improved by flying an appropriate trajectory. Our analysis

assumes a focused system, in which the radar returns from the scatterers are phase corrected for coherence.

The main factors impacting on the generation of appropriate trajectories have been discussed earlier. Note that imaging the target using DBS is not permissible for the whole of the terminal engagement and some means of homing in on the target at short ranges is required. This issue is not addressed in this paper. The derivation of the DBS equations makes use of some basic radar formulae. The Doppler shift from a point on the ground is given as:

$$f_D = \frac{2(\mathbf{v}.\mathbf{R})}{\lambda}. \tag{56}$$

where $\mathbf{R}$ is a unit vector aligned with the sightline axis and $\mathbf{v}$ is a vector aligned with a wind axes set. Using the transformation matrices, the velocity vector and the unit sightline vector can be written, in terms of space orientated unit vectors $(\mathbf{i}, \mathbf{j}, \mathbf{k})$ as:

$$\mathbf{v} = V\left(c(\gamma)c(\chi)\mathbf{i} + \ c(\gamma)s(\chi)\mathbf{j} + s(\gamma)\mathbf{k}\right) \tag{57}$$

$$\mathbf{R} = c(\lambda_y)c(\lambda_z)\mathbf{i} + c(\lambda_y)s(\lambda_z)\mathbf{j} - s(\lambda_z)\mathbf{k}. \tag{58}$$

The vector dot product can be written:

$$\mathbf{v}.\mathbf{R} = |\mathbf{v}||\mathbf{R}| \ cos(\Omega). \tag{59}$$

Where Ω is the total angle between the velocity vector and the sightline vector. Hence:

$$\mathbf{v}.\mathbf{R} = Vcos(\Omega) \tag{60}$$

$$\Omega = c^{-1}\left(c(\lambda_z)c(\lambda_y)c(\gamma)c(\chi) + c(\gamma)s(\chi)c(\lambda_y)s(\lambda_z) - s(\gamma)s(\lambda_y)\right) \tag{61}$$

$$f_D = \frac{2Vcos(\Omega)}{\lambda}. \tag{62}$$

The total angle between the velocity vector and the sightline vector can be expressed as:

$$cos(\Omega) = cos(\Xi)cos(\Lambda). \tag{63}$$

Now consider two points on the ground (A and B say) that need to be resolved in Doppler. Since the range to these points is different, and the missile is travelling at velocity V, the Doppler shift at these points will be:

$$f_{DA} = \frac{2Vcos(\Xi)cos(\Lambda)}{\lambda} \tag{64}$$

$$f_{DB} = \frac{2Vcos(\Xi + \delta\Xi)cos(\Lambda)}{\lambda}. \tag{65}$$

Subtracting the Doppler difference gives:

$$\Delta f_D = \frac{2V\ cos(\Lambda)\,(cos(\Xi) - cos(\Xi)cos(\delta\Xi) + sin(\Xi)\sin(\delta\Xi))}{\lambda} \tag{66}$$

$$\Delta f_D \approx \frac{2V\ cos(\Lambda)sin(\Xi)\delta\Xi}{\lambda} \quad for\ small\ \delta\Xi. \tag{67}$$

The Doppler resolution in crossrange is given by:

$$\frac{1}{\delta t} = \frac{2V\,(cos(\Lambda)sin(\Xi)\delta\Xi)}{\lambda}. \tag{68}$$

Rearranging yields:

$$\delta\Xi = \frac{\lambda}{2(V)(\delta t)\ sin(\Xi)cos(\Lambda)}. \tag{69}$$

The crossrange resolution (Δ) is the product of the range (R) and the increment in azimuth angle between the velocity vector and sightline vector:

$$\Delta = R(\delta\Xi) = \frac{R\ \lambda}{2V(\delta t)sin(\Xi)cos(\Lambda)}. \tag{70}$$

In terms of the terminal guidance problem it can be seen that the crossrange resolution is inversely proportional to the azimuth angle between the velocity vector and sightline (Ξ). An important fact to note is that the angle (Ξ) will approach zero as the velocity and sightline vectors become aligned.

Now assume that the target has been acquired prior to the terminal guidance phase. This is shown in Figure 9; it is assumed the target lies at ground level. Four frames of reference are shown on in Figure 9:

1. Earth fixed frame (X_S, Y_S, Z_S)
2. Missile body frame (X_B, Y_B, Z_B)
3. Missile inertial frame (X_I, Y_I, Z_I)
4. Sightline frame (X_A, Y_A, Z_A).

It is assumed that the missile inertial frame and earth fixed frame are aligned with one another. We consider the engagement in the azimuth plane only in order to derive a simplified expression for the crossrange resolution. The simplified expression is used purely for optimization purposes, needless to say in the figures where crossrange resolution is displayed the correct expression

(70) is used. The simplified expression is exact for flight parallel to the x-axis and zero elevation angle between the velocity vector and sightline (i.e. an azimuth plane engagement with flight along the x-axis). If we consider a planar engagement in the azimuth plane only equation (70) simplifies to:

$$\Delta = \frac{\lambda(\sqrt{x^2+y^2})}{2V(\delta t)\ sin(\Xi)}. \tag{71}$$

Now

$$\Xi = \lambda_y - \chi \tag{72}$$

$$sin(\lambda_y - \chi) = sin(\lambda_y)cos(\chi) - cos(\lambda_y)sin(\chi). \tag{73}$$

From Figure 9:

$$sin(\lambda_y) = \frac{y}{\sqrt{x^2+y^2}} \tag{74}$$

$$cos(\lambda_y) = \frac{x}{\sqrt{x^2+y^2}} \tag{75}$$

$$cos(\chi) = \frac{V_{sx}}{Vcos(\gamma)} \tag{76}$$

$$sin(\chi) = \frac{V_{sy}}{Vcos(\gamma)}. \tag{77}$$

Substituting gives:

$$\Delta = \frac{\lambda(x^2+y^2)}{2(\delta t)\,(V_{sx}(y) - V_{sy}(x))}. \tag{78}$$

For small (χ) the following approximations are valid:

$$V \approx V_{sx}, V_{sy} \approx 0.0. \tag{79}$$

Hence the crossrange resolution simplifies to:

$$\Delta = \frac{\lambda(x^2+y^2)}{2V(\delta t)(y)}. \tag{80}$$

10 References

[1] Kim, E., Cho, H., and Lee, Y., "Terminal Guidance Of Missiles Maneuvering In The Vertical Plane", *AIAA Guidance, Navigation And Control Conference*, San Diego, California, July 1996.

[2] Kim, M., and Grider, K. V., "Terminal Guidance for Impact Attitude Constrained Flight Trajectories", *IEEE Transactions On Aerospace And Electronic Systems*, Vol AES-9, No.6, November 1973.

[3] Green, M. and Limebeer, D. J. N., *Linear Robust Control*, Prentice Hall International, 1995.

[4] Song, T. L., and Shin, S. J., "Time Optimal Impact Angle Control for Vertical Plane Engagements", *IEEE Transactions on Aerospace and Electronic Systems*, Vol 35, No. 2, April 1999.

[5] Nasuti, F., and Innocenti, M., "Missile Trajectory Optimization With Agility Issues", *AIAA Guidance, Navigation And Control Conference*, San Diego, California, July 1996.

[6] Kumar, R., Seywald, H., Cliff, E., and Kelley, H. J. M, "Three Dimensional Air-to-Air Missile Trajectory Shaping", *Journal of Guidance, Control and Dynamics*, Vol. 18, No. 3, May-June 1995.

[7] Kumar, R., Seywald, H., and Cliff, E., "Near Optimal Three-Dimensional Guidance Against Maneuvering Target", *Journal of Guidance, Control and Dynamics*, Vol. 18, No. 3, May-June 1995.

[8] Lu, P., and Pierson, B. L., "Optimal Aircraft Terrain-Following Analysis and Trajectory Generation", *Journal of Guidance, Control and Dynamics*, Vol.18, No.3, May-June 1995.

[9] Menon, P. K. A, Kim, E., and Cheng, V. H. L., "Optimal Trajectory Synthesis for Terrain-Following Flight", *Journal of Guidance, Control and Dynamics*, Vol.14, No.4, July-August 1991.

[10] Lu, P., and Pierson, B. L., "Aircraft Terrain-Following Based on a Nonlinear Continuous Predictive Control Approach", *Journal of Guidance, Control and Dynamics*, Vol.18, No.1, July-August 1995.

[11] Grimm, W., and Hiltmann, P., "Direct And Indirect Approach For Real-Time Optimization Of Flight Paths", *Proceedings of the Conference on Optimal Control and Variational Calculus*, Oberwolfach, West-Germany, June 15-21, 1986, Lecture Notes in Control and

Information Sciences, Edited by R. Bulirsch, A. Miele, J. Stoer and K. H. Well, Springer Verlag, 1987.

[12] Betts, J. T., "Sparse Jacobian Updates in the Collocation Method for Optimal Control Problems", *Journal of Guidance, Control and Dynamics*, Vol. 13, No. 3, May-June 1990.

[13] Skalecki, L., and Martin, M., "Application of Multiple Shooting to Closed Loop Guidance", IAF Paper 91-326, *42nd Congress of the International Astronautical Federation*, October 1991.

[14] Skalecki, L., and Martin, M., "General Adaptive Guidance Using Nonlinear Programming Constraint-Solving Methods",*Journal of Guidance, Control and Dynamics*, Vol. 16, No. 3, May-June 1993.

[15] Kumar, R., and Seywald, H., "Dense-Sparse Discretization for Optimization and Real-Time Guidance", *Journal of Guidance, Control and Dynamics*, Vol 19, No. 2, p501-503.

[16] Garnell, P., and East, D., *Guided Weapon Control Systems*, Pegamon Press, 1977.

[17] Pytlak, R., and Vinter, R. B., "A Feasible Directions Type Algorithm For Optimal Control Problems With Hard State And Control Constraints", *IEEE Proceedings Of The 32nd Conference On Decision And Control*, San Antonio, Texas, December 1993, p3335-3340.

[18] Pytlak, R., and Vinter, R . B., "A Feasible Directions Algorithm For Optimal Control Problems With State And Control Constraints: Implementation", *Journal Of Optimization Theory and Applications*, 191, 1999, p623-649.

[19] Pytlak, R., and Vinter, R . B., "Second Order Method For Optimal Control Problems With Hard State And Control Constraints", *IEEE Proceedings Of The 34th Conference On Decision And Control*, New Orleans, December 1995.

[20] Pytlak, R., and Vinter, R. B., "A Feasible Directions Type Algorithm For Optimal Control Problems With Hard State And Control Constraints," *Proceedings of the 32nd Conference on Decision and Control*, San Antonio, Texas, December 1993, pp. 3335-3340.

[21] Pytlak, R., " *Numerical Methods for Optimal Control Problems with State Constraints*, Springer-Verlag, Lecture Notes in Mathematics, 1707"

[22] Minzner, R. A., Champion, K. S. W., and Pond, H. L., "*The ARDC Model Atmosphere*", Air Force Cambridge Research Centre, Bedford, MA, 1959.

[23] Hovanessian, S. A. , *Radar Detection And Tracking Systems*, Artech House, Inc, Dedham, Massachusetts, 1983.

[24] Edde, B., *Radar : Principles, Technology and Applications*, Prentice Hall, 1993.

[25] Franceschetti, G., and Lanari, R., *Synthetic Aperture Radar Processing*, CRC Press, 1999.

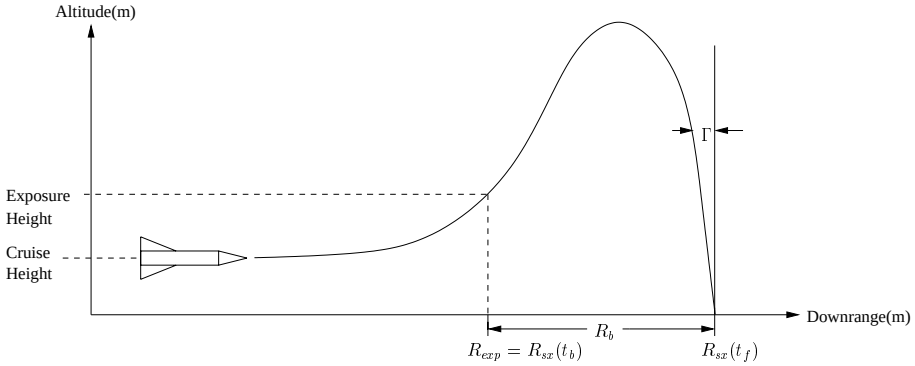

Figure 1: Bunt maneuver definitions

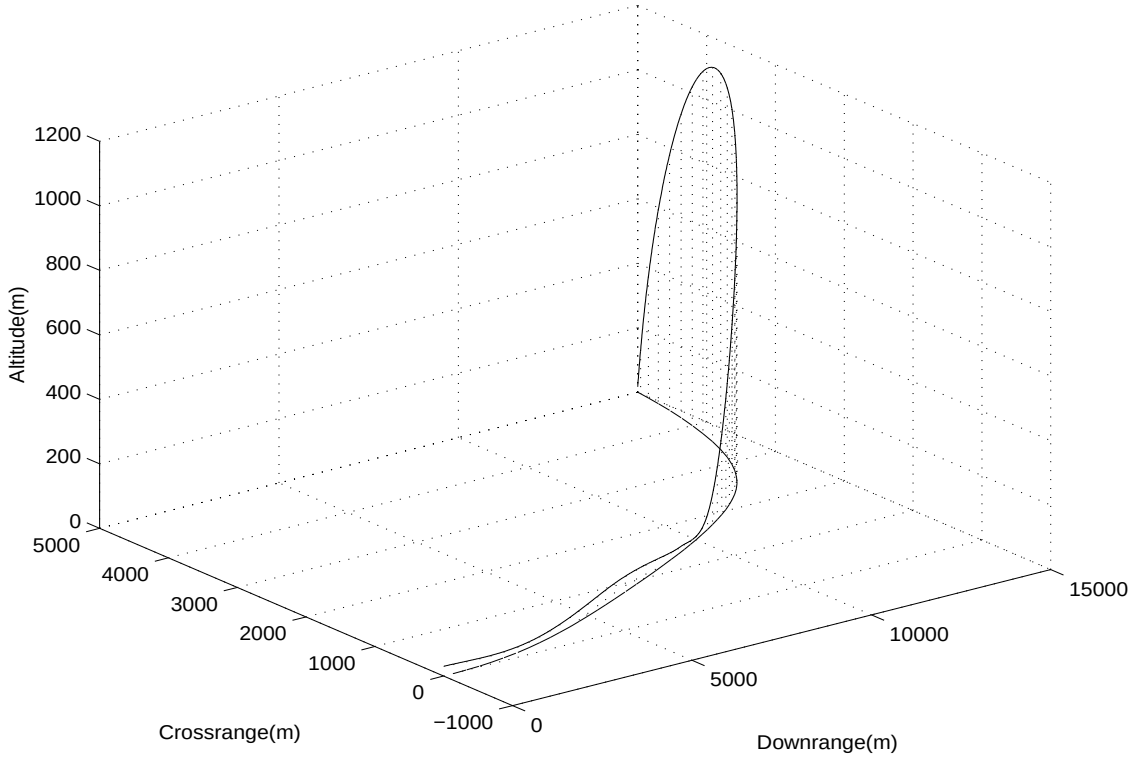

Figure 2: 3D Trajectory for Case A

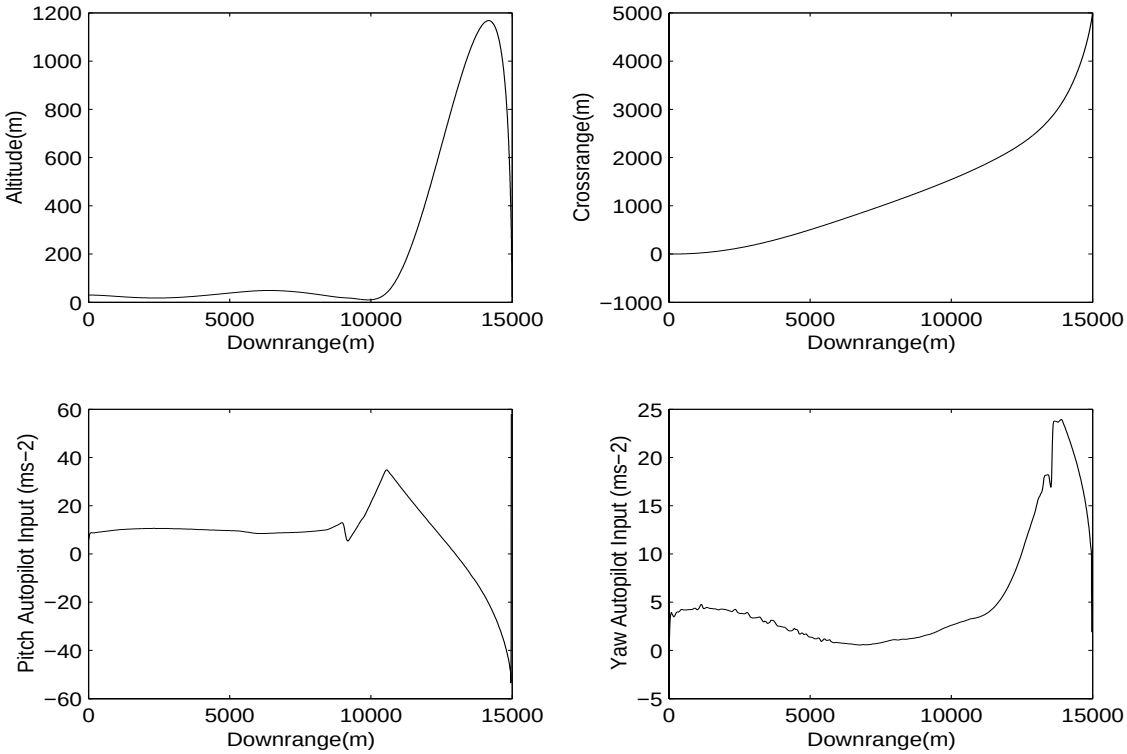

Figure 3: States and controls for Case A

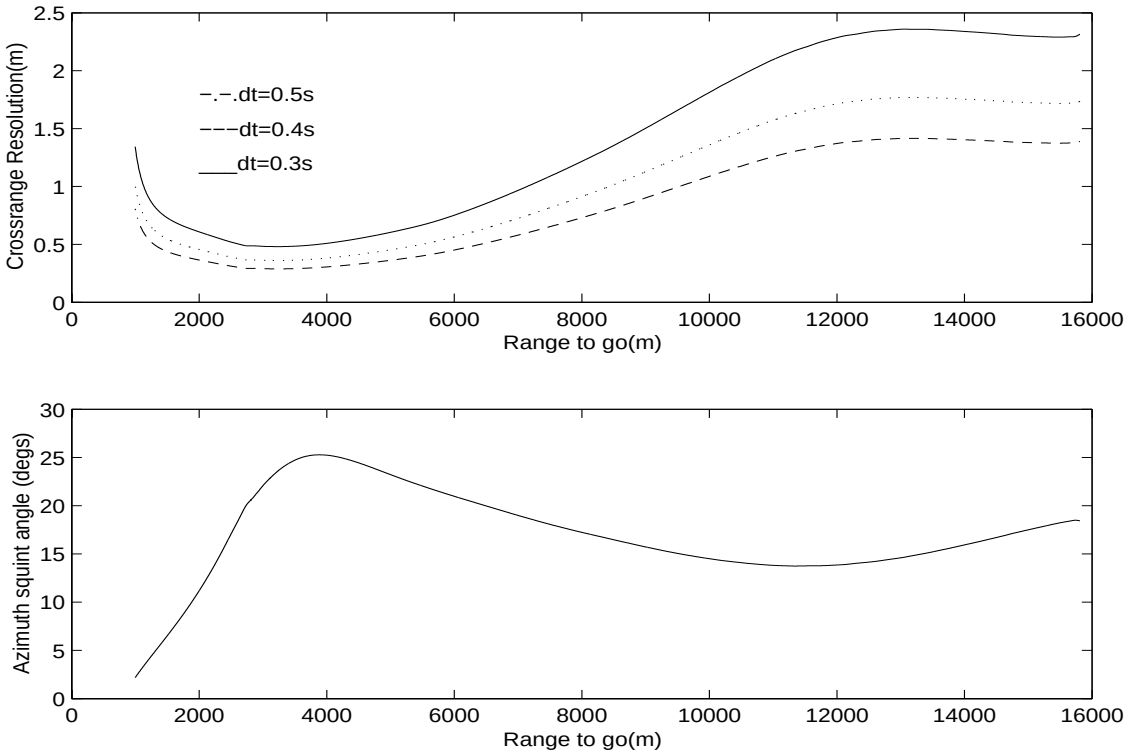

Figure 4: Crossrange resolution and azimuth angle for Case A

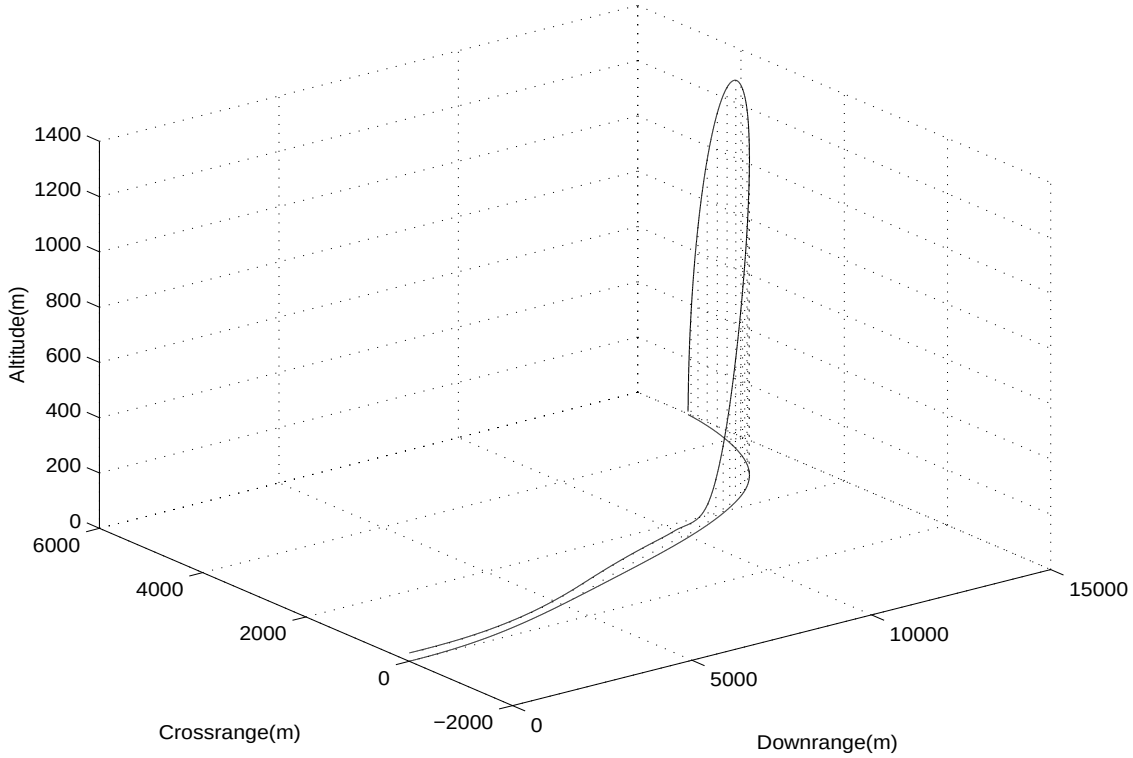

Figure 5: 3D Trajectory for Case B

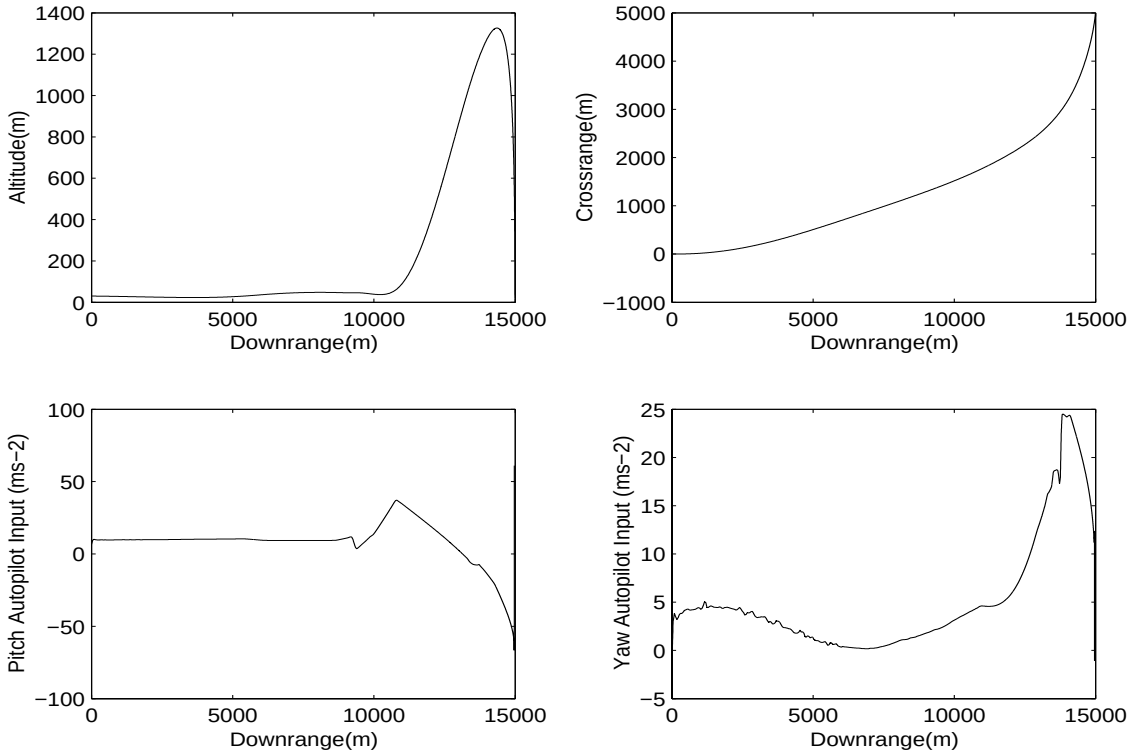

Figure 6: States and controls for Case B

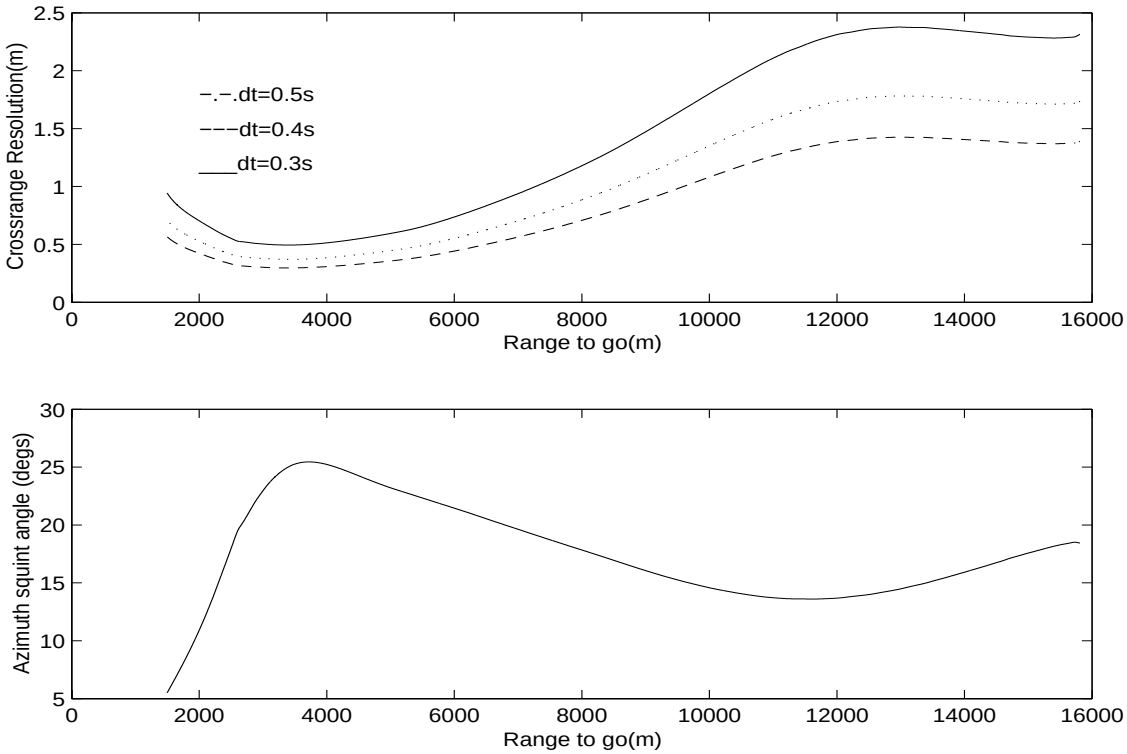

Figure 7: Crossrange resolution and azimuth angle for Case B

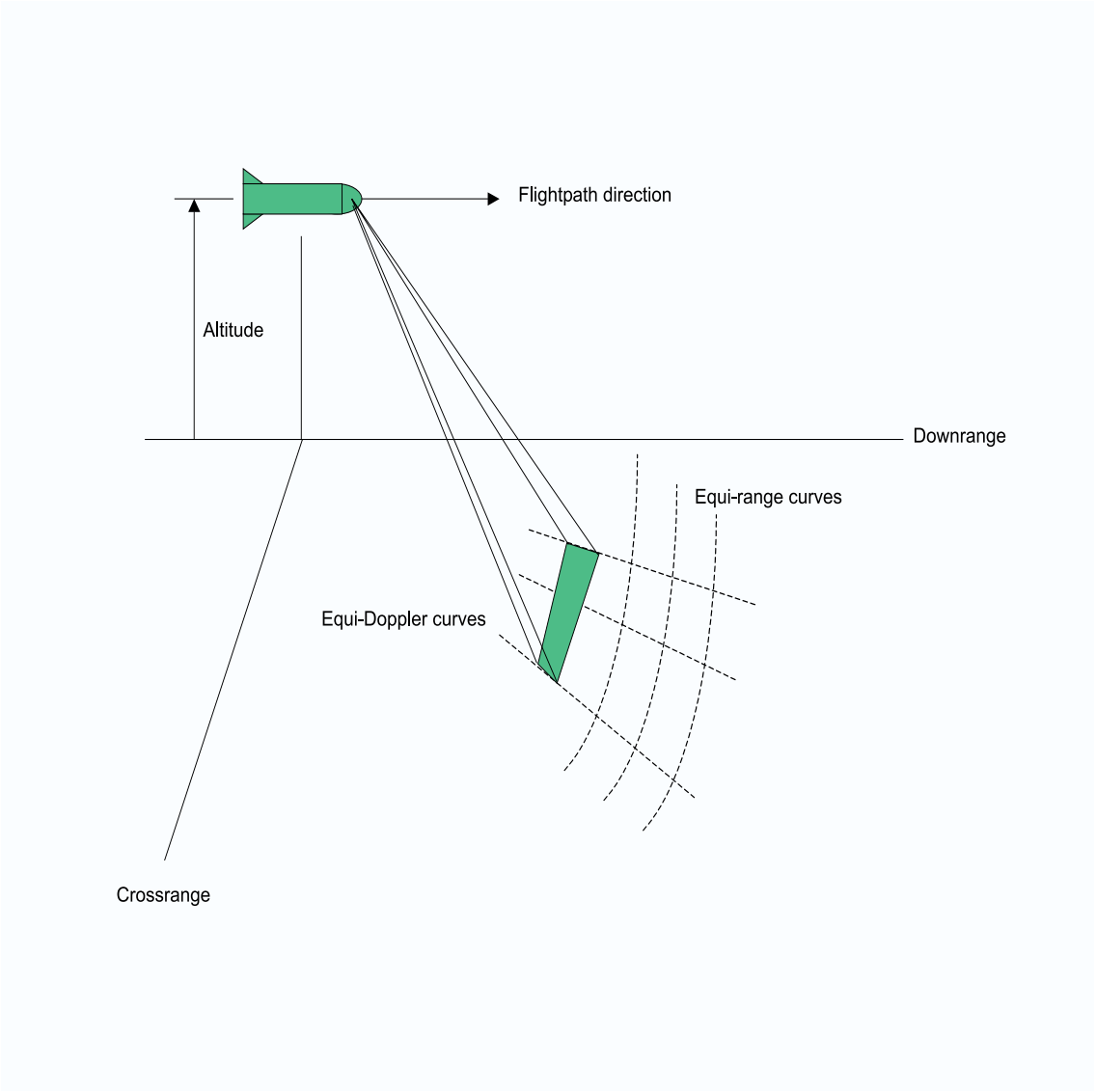

Figure 8: DBS radar

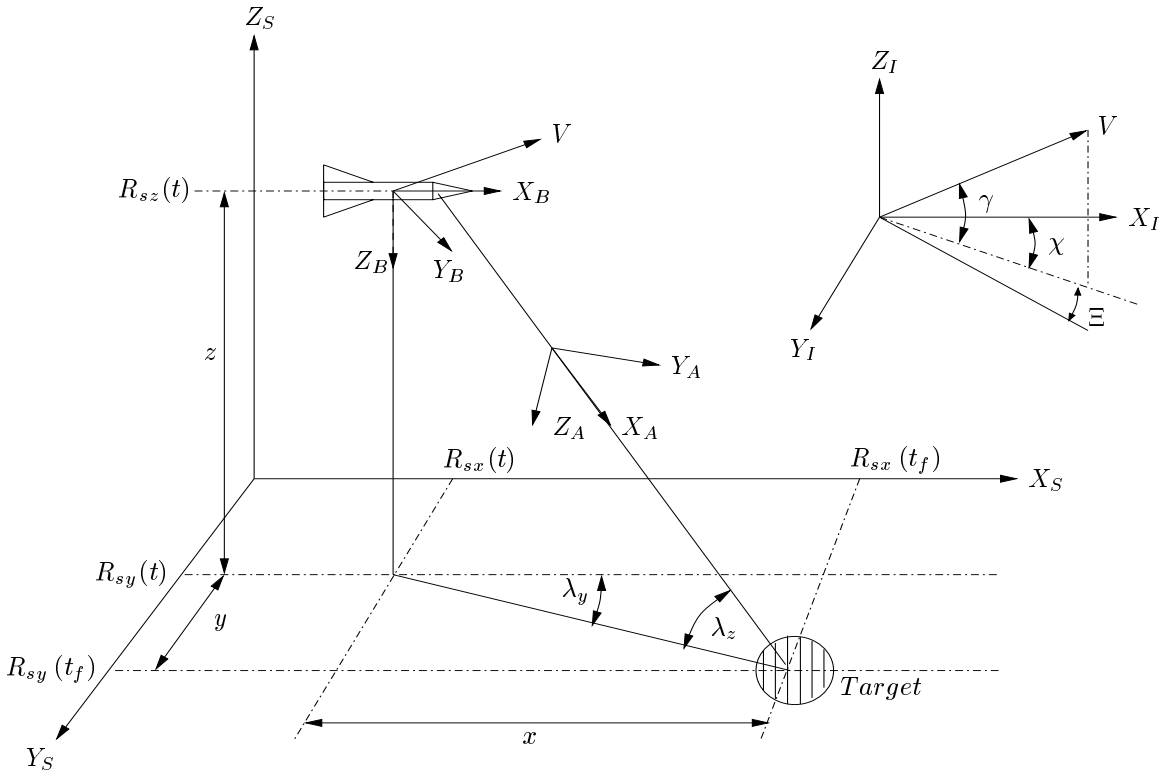

Figure 9: DBS terminal guidance